A Journal of the Gesellschaft Deutscher Chemiker

Angewandte International Edition GDCh Chemie

www.angewandte.org

Accepted Article

Title: Metal-Free Photocatalytic CO2 Reduction to CH4 and H2O2 under Non-sacrificial Ambient Conditions

Authors: Weixin Zou, Yingyi Cheng, Yu-Xin Ye, Xiaoqian Wei, Qing Tong, Lin Dong, and Gangfeng Ouyang

To be cited as: *Angew. Chem. Int. Ed.* **2023**, e202313392

Link to VoR: https://doi.org/10.1002/anie.202313392

WILEY VCH

10.1002/anie.202313392

WILEY VCH

RESEARCH ARTICLE

Metal-Free Photocatalytic CO_2 Reduction to CH_4 and H_2O_2 under Non-sacrificial Ambient Conditions

Weixin Zou,[a] Yingyi Cheng,[b] Yu-Xin Ye,*[c] Xiaoqian Wei,[a] Qing Tong,*[a] Lin Dong,[a] Gangfeng Ouyang*[b] [c]

[a] Dr. W. Zou, X. Wei, Dr. Q. Tong, Prof. L. Dong
State Key Laboratory of Pollution Control and Resource Reuse, School of the Environment, Jiangsu Key Laboratory of Vehicle Emissions Control, Center of Modern Analysis
Nanjing University
Nanjing 210023 (P. R. China)
E-mail: tongqing@nju.edu.cn

[b] Y. Cheng, Prof. G. Ouyang
Key Laboratory of Bioinorganic and Synthetic Chemistry of Ministry of Education, LIFM, School of Chemistry, IGCME
Sun Yat-sen University
Guangzhou 510006 (P. R. China)
E-mail: cesoygf@mail.sysu.edu.cn

[c] Dr. Y. -X. Ye, Prof. G. Ouyang
School of Chemical Engineering and Technology, IGCME
Sun Yat-sen University
Zhuhai 519082 (P. R. China)
E-mail: yeyuxin5@sysu.edu.cn

Abstract: Photocatalytic CO_2 reduction to CH_4 requires photosensitizers and sacrificial agents to provide sufficient electrons and protons through metal-based photocatalysts, and the separation of CH_4 from by-product O_2 has poor applications. Herein, we successfully synthesize a metal-free photocatalyst of a novel electron-acceptor 4,5,9,10-pyrenetetrone (PT), to our best knowledge, this is the first time that metal-free catalyst achieves non-sacrificial photocatalytic CO_2 to CH_4 and easily separable H_2O_2. This photocatalyst offers CH_4 product of 10.6 $\mu mol \cdot g^{-1} \cdot h^{-1}$ under non-sacrificial ambient conditions (room temperature, and only water), which is two orders of magnitude higher than that of the reported metal-free photocatalysts. Comprehensive *in situ* characterizations and calculations reveal a multi-step reaction mechanism, in which the long-lived oxygen-centered radical in the excited PT provides as a site for CO_2 activation, resulting in a stabilized cyclic carbonate intermediate with a lower formation energy. This key intermediate is thermodynamically crucial for the subsequent reduction to CH_4 product with the electronic selectivity of up to 90%. The work provides fresh insights on the economic viability of photocatalytic CO_2 reduction to easily separable CH_4 in non-sacrificial and metal-free conditions.

Introduction

The utilization of carbon dioxide (CO_2) to produce valuable chemicals as alternative fuels could lower the net costs of decreasing emissions of CO_2 to the atmosphere.[1] Photocatalytic CO_2 reduction has been considered a sustainable approach to the production of green fuels.[2,3] Among the energy-rich C1 products, methane (CH_4) is provided with the highest combustion heat value of 890 $kJ \cdot mol^{-1}$, while methanol, formaldehyde, carbon monoxide, and formic acid have only 727, 571, 283, and 254 $kJ \cdot mol^{-1}$, respectively. In addition, CH_4 is also the cleanest hydrocarbon fuel and is used as a hydrogen carrier. However, to date, the current photocatalytic synthesis systems for CH_4 product is still hard to construct. One of the main reasons is the low methanation selectivity of the reduction half-reaction, because the electrochemical potentials of various CO_2 reduction products are very close to CH_4, *i.e.* -0.53 V for CO, -0.61 V for HCOOH, -0.38 V for CH_3OH, and -0.24 V for CH_4 vs normal hydrogen electrode (NHE).[4,5] Moreover, CH_4 is produced by multi-step reactions with eight electrons, while CO ($2e^-$), HCOOH ($2e^-$), and CH_3OH ($6e^-$) are all kinetically superior competing products, so the methanation reaction may terminate at one of the intermediate steps, resulting in no CH_4 product.[6] In addition, the separation of CH_4 from the by-product O_2 in the oxidation half-reaction has poor sustainability and economic viability, and the evolution of liquid rather than gaseous by-products is meaningful, where the separation costs and environmental problems can be avoided.

To achieve a highly selective half-reaction of the CH_4 product, complex or metal co-catalysts as active sites were necessary.[7,8] A few complex active sites could effectively improve the selectivity of CH_4, *i.e.* low-valent iron, cobalt, and copper metal centers. Also, co-catalysts such as Ni, Ru, Re, Rh, and Co, or noble metals like Au or Pt, lead-halide perovskite quantum dots, or metal oxides act as active sites for methanation.[9-14] The highly selective CH_4 product of these metal active sites is attributed to the strong coordination between CO and metal sites to convert the *CO intermediate to further reduction products. However, the above catalytic active center often requires expensive sacrificial electron donors, molecular photosensitizers, or semiconductors to provide electrons and protons to initiate the reaction, because it is quite difficult to achieve another half-reaction of water oxidation. Furthermore, the limited metal resources in photocatalysts could result in higher methanation costs and hinder a wider application.

Metal-free organic polymeric materials consist of renewable and cheap resources with facile modulation of physicochemical properties.[15] The atomic-level tunability of their backbone

10.1002/anie.202313392

enables the targeted introduction of active sites by rational backbone engineering. For example, a redox-active conjugated microporous polymer showed intramolecular charge-transfer-assisted photocatalytic CO_2 reduction to CH_4.[16] Recently, it has been reported a transition-metal-free catalyst system for the photocatalytic CO_2 reduction and the formate product was obtained.[17] However, the current work on metal-free materials for CO_2 reduction usually uses photosensitizers or sacrificial agents to provide enough electrons and protons for the highly selective CH_4 evolution.[11,13,16,17] Due to organic materials with a weaker ability than inorganic materials to obtain electrons from water, as well as more electrons required for the CH_4 product, the ability of metal-free organic materials to provide sufficient electrons to the active center for CO_2 photoreduction to CH_4 is still difficult.

Herein, we have successfully constructed a novel metal-free photocatalyst containing an electron-acceptor 4,5,9,10-pyrenetetrone (PT) and electron-donor tetraphenyl ethylene (TPE) as active sites for CO_2 and H_2O, respectively, to produce CH_4 and H_2O_2, using renewable solar energy under non-sacrificial ambient conditions (room temperature and only water), and this system exhibits the following advantages: (1) The relatively cheap CO_2 and H_2O feedstocks produce a higher combustion-value CH_4. (2) The by-product H_2O_2 is in the liquid phase, which is easy to separate from the gaseous CH_4, compared with O_2. (3) The metal-free photocatalysts are made from elements that are abundant on Earth. (4) No electron donors or high-energy inputs are needed with environmental sustainability and economic viability. Under the non-sacrificial ambient conditions, the photocatalytic CH_4 production rate was 10.6 $\mu mol \cdot g^{-1} \cdot h^{-1}$ with up to 90% electronic selectivity under ambient conditions. To our best knowledge, this is the first time that non-sacrificial photocatalytic CO_2 via H_2O to CH_4 and H_2O_2 has been achieved by a metal-free catalyst. Systematic investigations demonstrated that the long-lived oxygen-centered radical in photoexcited PT presented as an active site for CO_2 activation, which generated a cyclic 1,3-dioxolan-2-one intermediate to stabilize *CO that was thermodynamically crucial for CH_4 product. In addition, the weak adsorption between H_2O and TPE/alkynyl facilitated the proton migration for highly selective production of CH_4. Furthermore, owing to the strong electron-withdrawing capacity of PT, abundant electrons were provided for the CH_4 product with ultrafast electron extraction in 161 ps under a CO_2 atmosphere. The study could open the door to the potential of organic active sites as sustainable protocols for non-sacrificial photocatalytic CH_4 generation.

Results and Discussion

Structures of Metal-Free Photocatalysts

The electron donor-acceptor (D-A) photocatalyst was synthesized with TPE as an electron-donor, PT as an electron-acceptor, and alkynyl as a connector, named TPE-PT (Figure 1a). For comparison, analogous D-A conjugated polymers of TPE-anthraquinone (AQ) with AQ as an electron-acceptor, and triphenyl triazine (TPT)-AQ with TPT as an electron-donor and AQ as an electron-acceptor were also synthesized. All these three photocatalysts were synthesized through a one-step Sonogashira reaction.[18]

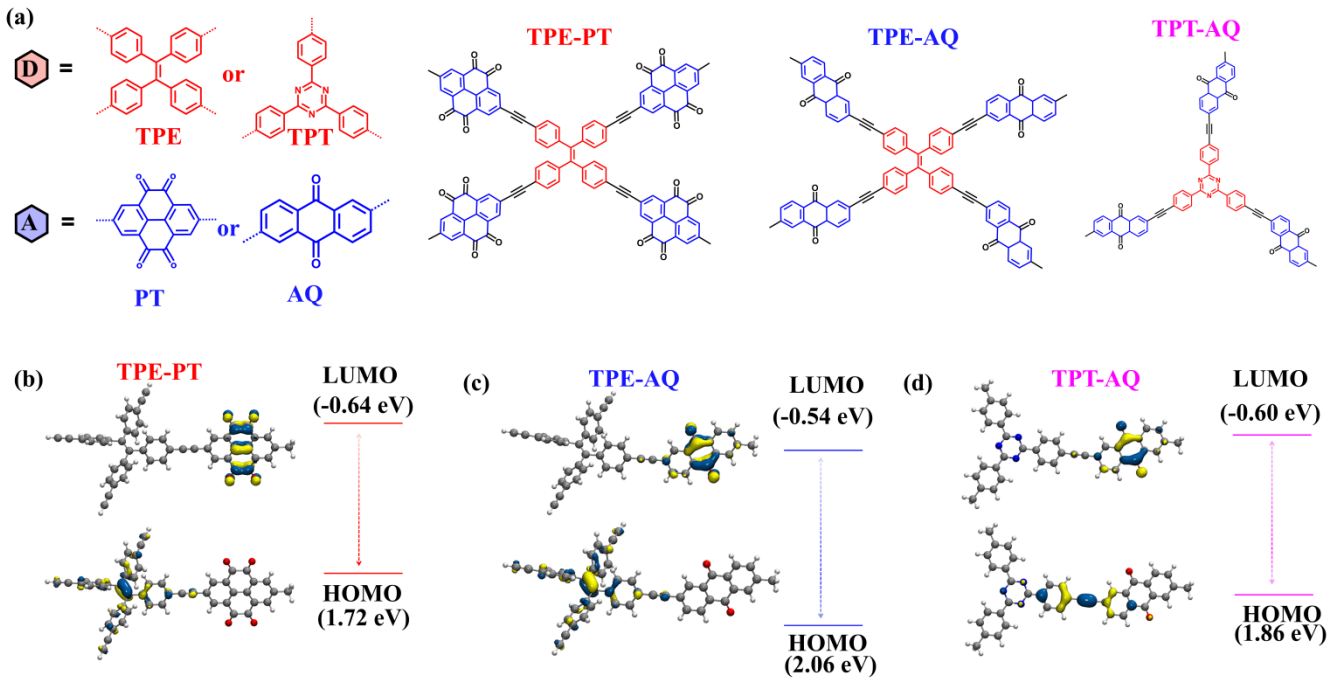

Figure 1. (a) The molecular structures of the electron D-A conjugated polymers. The charge distributions calculated by the density functional theory (DFT) method and band structures for (b) TPE-PT, (c) TPE-AQ, (d) TPT-AQ. TPE or TPT moieties exhibited electron-offering ability as the highest occupied molecular orbital (HOMO), and PT or AQ moieties exhibited electron-accepting ability as the lowest unoccupied molecular orbital (LUMO) of these polymers.

10.1002/anie.202313392

RESEARCH ARTICLE

The powder X-ray diffraction (PXRD) profiles revealed that all photocatalysts exhibited the feature of amorphous carbon (Figure S1).[19] The scanning electron microscopy (SEM) photos indicated the photocatalysts were bulky structures (Figure S2). The transmission electron microscope (TEM) and related mapping photos demonstrated the photocatalysts were exfoliated structures with a uniform distribution of carbon and oxygen over the photocatalysts (Figure S3). The solid-state ^{13}C nuclear magnetic resonance (NMR), X-ray photoelectron spectroscopy (XPS), Fourier transform infrared spectra (FT-IR), and Raman characterizations determined the photocatalyst structure. The solid-state ^{13}C NMR spectra (Figure S4a) showed that peaks displayed for keto carbons at ~180 ppm (C=O), aromatic carbons at ~120-140 ppm (C=C), and alkyne carbons at ~90 ppm (C≡C),[16] and the XPS spectra (Figure S4b and S4c) suggested the existence of C≡C (283.5 eV), aromatic carbon (284.8 eV), and C=O (289.0, and 532.4 eV). Additionally, characteristic alkynyl groups at ~2300 cm^{-1} and C=O stretching bands at ~1700 cm^{-1} [20] in FT-IR (Figure S4d) and Raman spectra (Figure S5) further proved the successful polymerization through the Sonogashira reaction for all the photocatalysts.[18] The Pd contents of TPE-PT, TPE-AQ, and TPT-AQ were 0.32, 0.19, and 0.35 wt% by ICP-OES analysis, respectively, and the XPS spectrum exhibited no obvious peak of Pd species (Figure S5), suggesting the very low content of Pd. Besides, the BET surface areas were shown in Table S1, and N_2 adsorption-desorption isotherms of all the photocatalysts suggested typical type-II loops with H3 or H4 hysteresis, showing that their similar microporous structures with ~0.4 nm (Figure S6).

All the photocatalysts exhibited strong absorption in the visible region (Figure S7), especially TPE-PT, which had strong absorption throughout the visible range, ascribed to its more π–π* transition of TPE units and intensive electronic push-pull effect. The conduction band minima (CBM) of TPE-PT, TPE-AQ, and TPT-AQ were characterized to be -0.64, -0.54, and -0.60 eV versus NHE via the Mott-Schottky tests (Figure 1b-d and S8).[20] Moreover, the valence band maxima (VBM) were calculated from valence band XPS (VB-XPS) and Kelvin probe force microscopy (KPFM). The VB-XPS and KPFM were used to determine the energy level difference from VBM to Fermi level, and Fermi level to vacuum level, respectively, which was subsequently converted from the vacuum level to the electrode potential (Figure S9 and S10). Therefore, the VBM of TPE-PT, TPE-AQ, and TPT-AQ were 1.72, 2.06, and 1.86 eV versus NHE, respectively (Figure 1b-d). All photocatalysts satisfied the potential requirements for CO_2 reduction to CH_4 and CO, and H_2O oxidation to O_2 or H_2O_2.

Non-sacrificial Photocatalytic CO_2 Reduction

The photocatalytic performance of CO_2 reduction was investigated. The CO_2 photoreduction test was conducted in a common gas-solid reactor under CO_2, water, and full spectrum illumination at room temperature. It was noted that no additional photosensitizers and sacrificial agents were added. Only CO and/or CH_4, traces of HCHO, and no H_2 or O_2 were detected as products. The highest CH_4 yield was observed in the TPE-PT sample, with 10.6 $\mu mol \cdot g^{-1} \cdot h^{-1}$ and as high as 90% electronic selectivity, which was nearly 9 times higher than that of TPE-AQ. No CH_4 was found in TPT-AQ (Figure 2a). In addition, TPE-PT can undergo at least five cycles without any decay in the performance (Figure 2b). The structural integrity of TPE-PT was retained after the reaction, confirmed by PXRD, and FT-IR (Figure S11). Compared to the metal-free and metal-contained materials under non-sacrificial and sustainable ambient conditions, the performance of TPE-PT was at the forefront (Figure 2c, Table S2).[21-28] Furthermore, the activity comparison between TPE-PT and other metal-free porous organic polymer-based materials for photocatalytic CO_2 reduction with only H_2O was shown in Table S3. Our production rate of CH_4 was much higher than those of reported metal-free photocatalytic conditions (two order of magnitude higher), not to mention that most of the reported product was CO, due to the weak interaction between *CO and metal-free active sites. Notably, our designed TPE-PT polymer exhibited the outstanding CH_4 yield and high selectivity for photocatalytic CO_2 reduction.

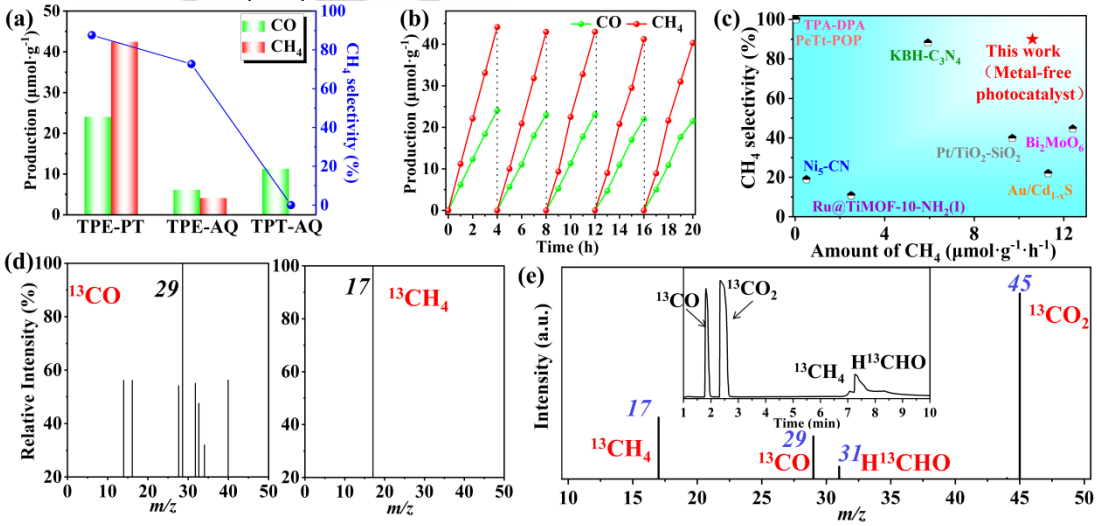

Figure 2. (a) The photocatalytic performances of CO_2 reduction of TPE-PT, TPE-AQ, and TPT-AQ, in a gas-solid reactor under CO_2 and water at room temperature for 4 h without additional photosensitizers or sacrificial agents. (b) Cycling tests of photocatalytic CO_2 reduction on TPE-PT for five runs. (c) The performances of photoreduction CO_2 to CH_4 in metal-free and metal-contained systems, without additional photosensitizers or sacrificial agents. (d) (e) The GC-MS spectra of products during photocatalytic CO_2 reduction involving $^{13}CO_2$ as a reactant.

10.1002/anie.202313392

RESEARCH ARTICLE

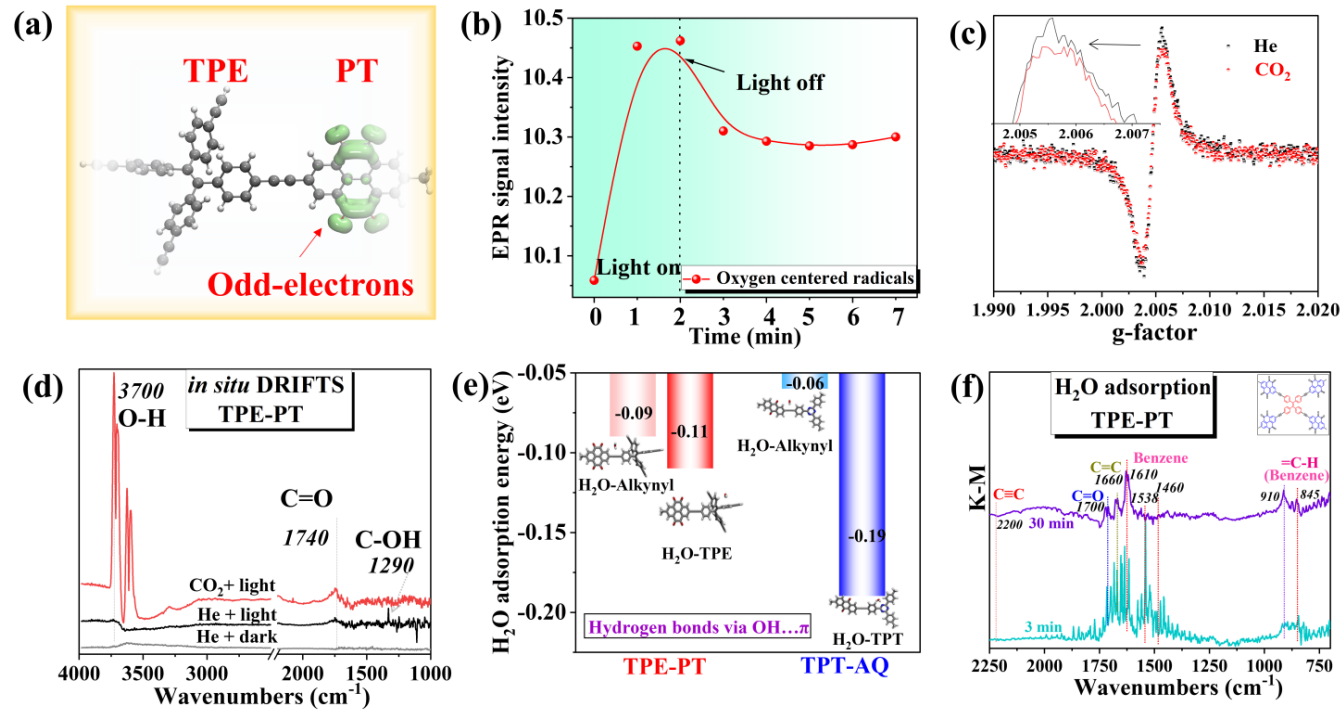

Figure 3. (a) The odd-electron density in a single TPE-PT unit through TD-DFT. (b) The EPR signal intensities with time of TPE-PT under light irradiation and afterward turning off light. (c) EPR spectra of TPE-PT under He or CO_2 conditions. (d) *In situ* DRIFTS in dark/light under He or CO_2 conditions of TPE-PT. (e) DFT calculations of H_2O adsorption energies. (f) *In situ* DRIFTS of H_2O adsorption in dark on TPE-PT.

^{13}C isotope labeling experiments were performed to ascertain the carbon sources of photocatalytic products (Figure 2d, e and S12). When a catalytic experiment was performed using ^{13}C-labeled CO_2 ($^{13}CO_2$) as the substrate, $^{13}CH_4$ (*m/z* = 17), ^{13}CO (*m/z* = 29), $H^{13}CHO$ (*m/z* = 31) were finally detected by the mass spectrometry, while no ^{12}CO (*m/z* =28) was detected, which confirmed that CH_4, CO, and HCHO production originated from the reactant CO_2, ruling out contributions from other carbon-containing species.

To achieve CO_2 photoreduction, another half-reaction of water oxidation reaction (WOR) in TPE-PT was crucial, and the potential oxidation by-products of gaseous O_2 and liquid H_2O_2 would have contrary economic costs of separation. Therefore, the rotating ring-disk electrode (RRDE) tests were conducted to clarify the exact oxidation products (Figure S13).[29] TPE-PT exhibited significant reduction currents when the applied potential at the Pt ring electrode was -0.64 V or +0.16 V *vs* NHE, which were attributed to O_2 and H_2O_2 as oxidation products, respectively. In the controlled experiments, a small amount of H_2O_2 (350 μmol·g^{-1}·h^{-1}) was detected in a CO_2-saturated aqueous solution, but no O_2 by-product was found during CO_2 photoreduction, probably due to further oxygen reduction reaction (ORR). Furthermore, the products of ORR were characterized by rotating disk electrode (RDE) voltammetry (Figure S14). The average electron transfer number involved in ORR was calculated to be 4.00 for TPE-PT, which was close to the theoretical value for directly and selectively reducing the generated O_2 into H_2O.

Therefore, CO_2 and H_2O conversion to CH_4 and H_2O_2 using renewable solar energy and metal-free photocatalysts in non-sacrificial ambient conditions (room temperature and only water) were achieved in TPE-PT, and the system featured excellent sustainability and economic viability of metal-free abundant elements, cheap CO_2 and H_2O feedstocks, large combustion-value CH_4 product without electron donors or high-energy inputs, and easy separation of CH_4 from by-product H_2O_2 liquid with circumventing O_2 generation.

Metal-Free Photocatalytic Mechanism

To further investigate the active sites for CO_2-to-CH_4 in a metal-free photocatalyst of TPE-PT, time-dependent DFT (TD-DFT) was adopted.[18] In Figure 3a, the excited odd-electrons were located in PT moieties. *In situ* electron paramagnetic resonance (EPR) described the photoexcitation radical to reveal an active site. Introducing light irradiation, the EPR signal (g = 2.0047) assigned to an oxygen-centered radical generated on PT in photoexcitation[30] was increased (Figure S15a). After turning off the light, the signal from PT slightly decreased and remained constant (Figure S15b). Additionally, the EPR signal intensities of oxygen-centered radicals with time were displayed in Figure 3b, it was suggested that the oxygen-centered radicals had a lifetime of over 5 minutes, and was more intensive than that observed before irradiation (Figure S15d), which was the potential to activate CO_2. Based on zooming the signal, a decline signal of the oxygen-centered radical was detected upon changing the gas condition from He to CO_2, serving as evidence that oxygen-centered radicals were employed in the capture and activation of CO_2, as shown in Figure 3c.

Furthermore, *in situ* diffuse reflectance infrared Fourier transform spectra (DRIFTS) under He or CO_2 conditions in dark/light (Figure 3d) confirmed the active site for CO_2 adsorption in TPE-PT. Peaks at 3700, 1740, and 1290 cm^{-1} were assigned to hydroxyl, carbonyl, and ring-based alcohol, respectively.[16,18]

10.1002/anie.202313392

RESEARCH ARTICLE

Compared spectra under He in dark and light, the peak intensities of hydroxyl, carbonyl, and ring-based alcohol increased in light, suggesting that photo-electrons transferred to carbonyls in PT, and reduced to hydroxyls and oxygen radicals. Subsequently, when He was switched to a CO_2 atmosphere in light, carbonyl species increased and ring-based alcohols decreased, indicating CO_2 activated on the ring-based alcohol of PT and further reduced to *COOH. Therefore, the photo-induced electrons transferred from TPE to PT moieties, and the carbonyls of PT reduced to hydroxyls and oxygen-centered radicals, which captured CO_2 and activated to *COOH species for initiating the CH_4 production, not the key *OCHO intermediate of HCOOH product.

The DFT calculations and *in situ* DRIFTS of H_2O adsorption explored the sites for H_2O oxidation in TPE-PT. The electron-donor (TPE) and photo-charge transfer bridge (alkynyl) acted as hole-aggregation sites for H_2O oxidation, and their corresponding adsorption energies (E_{ads}) for H_2O were calculated, respectively. The difference between $E_{ads,\ alkynyl}$ (-0.09 eV) and $E_{ads,\ TPE}$ (-0.11 eV) was not significant, compared with TPT site (Figure 3e), suggesting that H_2O oxidation occurred predominantly on benzene rings of TPE via hydrogen bonds of OH…π, partially on alkynyl sites. In addition, *in situ* DRIFTS of H_2O adsorption (Figure 3f) showed the peaks (1610, 1538, and 1460 cm^{-1}) of the benzene rings[31] occurred a noticeable change, suggesting H_2O dominantly adsorbed on benzene rings (TPE) via hydrogen bonds (OH…π), which then oxidized to H_2O_2 or O_2 by holes. It was also observed that the peak intensity of alkynyl (2200 cm^{-1}) slightly decreased, suggesting that alkynyl could act as another site for H_2O adsorption. Therefore, H_2O oxidation were on TPE and alkynyl sites. Afterward, the ORR would occur on C atoms (benzene rings near alkynyl), suggested by the calculated E_{ads} and *in situ* DRIFTS of O_2 adsorption (Figure S16).

The highly-selective CH_4 product was attributed to the strong coordination between *CO intermediates and active sites of PT, and easier proton migration of H_2O on TPE, therefore *in situ* DRIFTS were conducted to further detect the intermediates and reveal the mechanism for CO_2 reduction and H_2O oxidation. In Figure 4, both TPE-PT and TPT-AQ exhibited the characteristic peaks for *COOH intermediate (*ca.* 1360, 1510, 1600, 1720, and 3300 cm^{-1}), and monodentate carbonate m-CO_3^{2-} (*ca.* 1430 cm^{-1}).[32] On TPE-PT, in the light, m-CO_3^{2-} and *COOH intermediates were easier to generate and reduce. In addition, the peaks at 2080 and 1920 cm^{-1} (attributed to atop-absorbed *CO_{atop} and bridge-absorbed *CO_{bridge}, respectively,[32]) were observed, suggesting that the strong interaction between *CO and PT was conducive to protonation and reduction to *CHO (2720, and 1740 cm^{-1}) and *CH_3O (1120 cm^{-1}) intermediates.[26] While, on TPT-AQ, due to the intensive interaction between protons and TPT via C=NH^+ (1540 cm^{-1}),[31] consistent with the DFT results of E_{ads} for H_2O, *i.e.*,$E_{ads,\ alkynyl}$ (-0.06 eV) > $E_{ads,\ TPT}$ (-0.19 eV), the generated *COOH intermediate on TPT-AQ was harder to converse, and the decreased *CO intermediate suggested that the weaker interaction of *CO-AQ was easy to generate CO, and less *CHO intermediate and CH_4. As expected, peaks at 3030, 2980, 2930, and 2870 cm^{-1} ascribed to the asymmetric C-H stretching of CH_3 and CH_2 ($\nu_{as}(CH_3)$ and $\nu_{as}(CH_2)$), and symmetric C-H stretching of CH_3 and CH_2 ($\nu_s(CH_3)$ and $\nu_s(CH_2)$),[32] respectively, were only on TPE-PT, strongly supporting the formation of CH_4. Notably, the peak at about 1850 cm^{-1} assigned to C=O for cyclic ester was only observed in TPE-PT, proving that the cyclic carbonate was a key intermediate for the highly-selective CH_4 production.

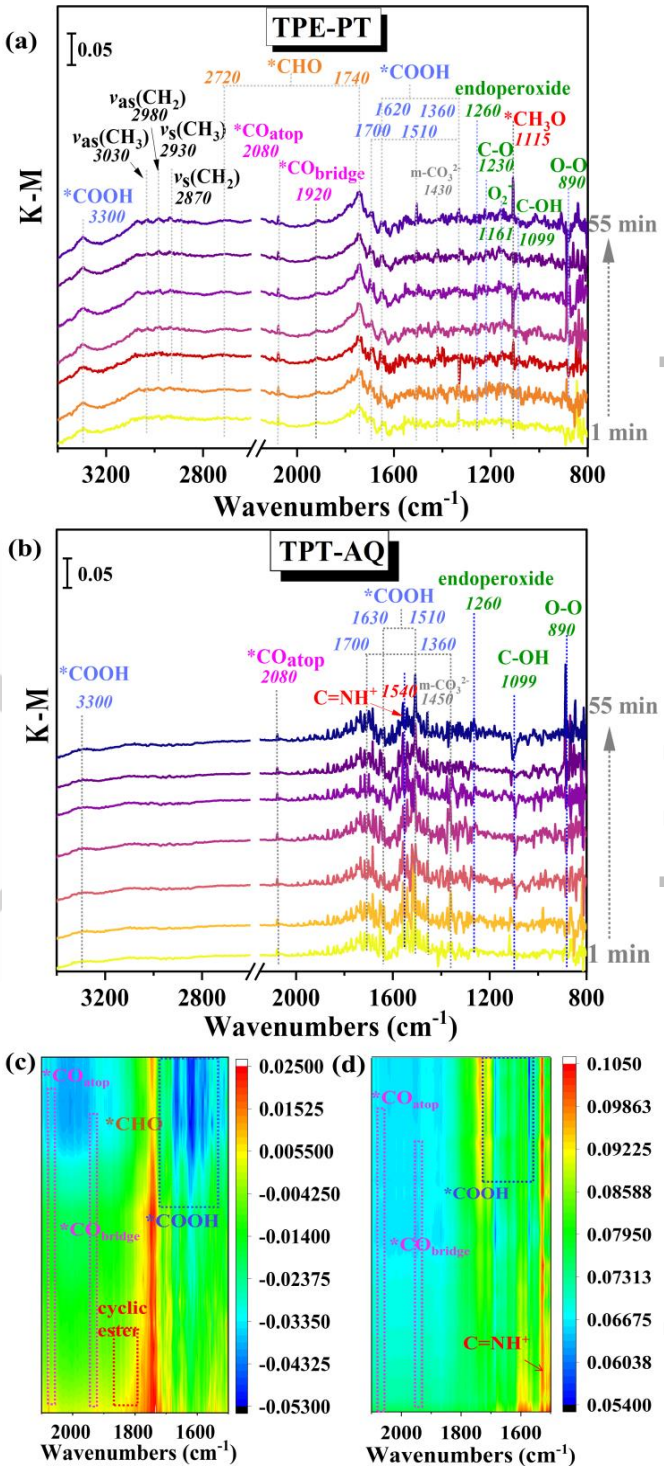

Figure 4. *In situ* DRIFTS of CO_2 and H_2O adsorption under light irradiation of (a) TPE-PT, and (b) TPT-AQ. The corresponding thermal maps in the range of 2100-1500 cm^{-1} of (c) TPE-PT, and (d) TPT-AQ.

In addition, on TPT-AQ, a stronger interaction of C=NH^+ (1540 cm^{-1}) was favorable for H_2O adsorption to C-OH (1099 cm^{-1}),[33] which was oxidized to H_2O_2, confirmed by the decreased peak of

10.1002/anie.202313392

RESEARCH ARTICLE

C-OH, and the increased peroxy (-O-O-) (890 cm^{-1}) and endoperoxide species (1260 cm^{-1}).[33] While, on TPE-PT, in the light irradiation, H_2O_2 was generated by the emerged peroxy (-O-O-) and endoperoxide species, and the O_2^- intermediate (1161 cm^{-1}) showed that the O_2 from partial H_2O oxidation further occurred reduction on C atom (1230 cm^{-1}).

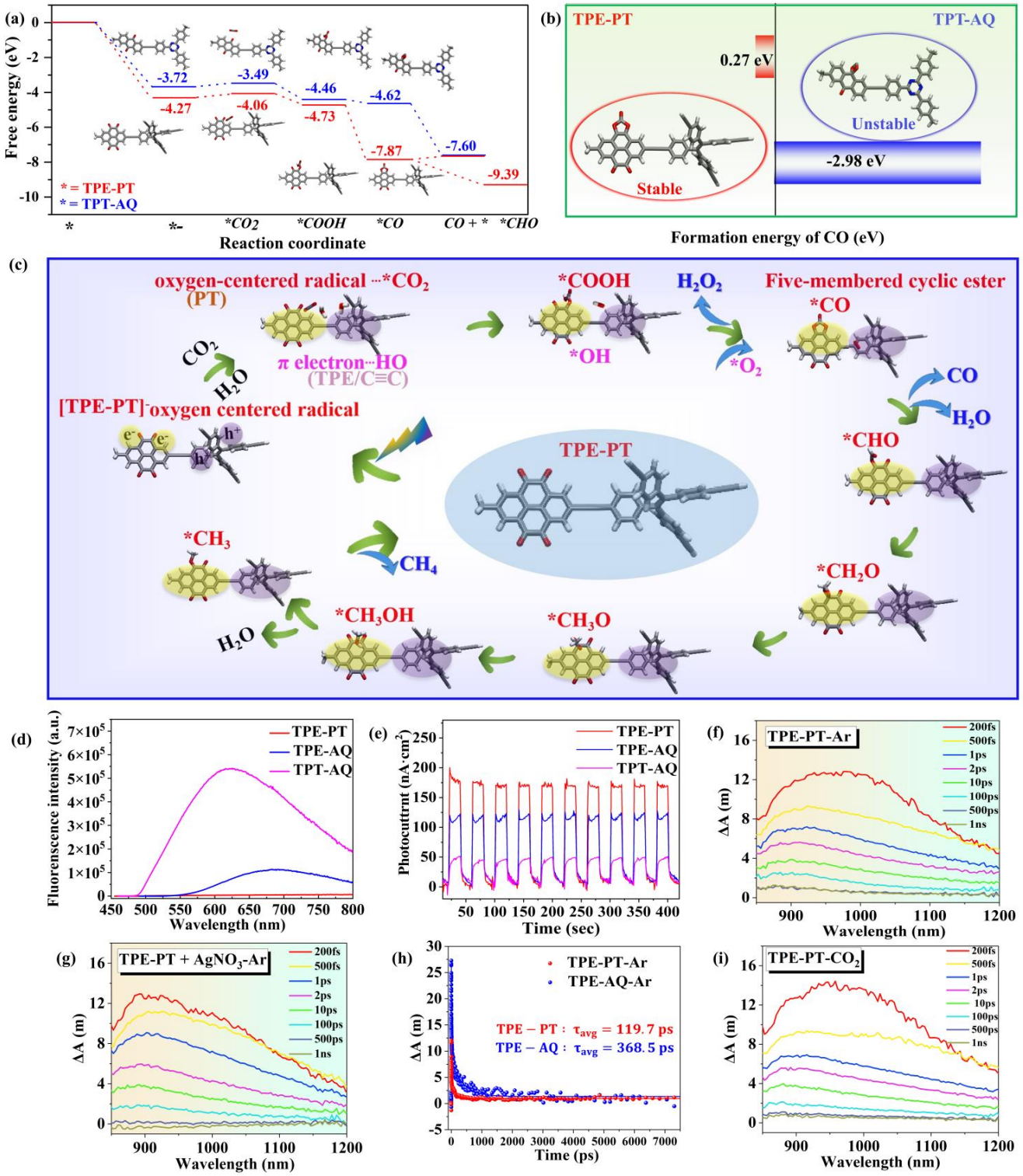

Figure 5. (a) Gibbs free energies of photocatalytic CO_2 reduction on TPE-PT and TPT-AQ. (b) Formation energies of CO on TPE-PT and TPT-AQ, respectively. (c) Proposed mechanism of CO_2 and H_2O conversion to CH_4 and H_2O_2 on TPE-PT under the light irradiation. (Red: oxygen, gray: carbon, white: hydrogen). (d) Photoluminescence spectra and (e) the transient photocurrent responses of TPE-PT, TPE-AQ and TPT-AQ. Femtosecond-transient absorption (fs-TA) spectra of TPE-PT in (f) Ar, and (g) Ar and $AgNO_3$ conditions, respectively. (h) TA kinetic traces of TPE-PT and TPE-AQ in Ar atmosphere. (i) fs-TA spectra of TPE-PT in CO_2 atmosphere.

The mechanism for the crucial intermediate generation was further investigated by the DFT calculations (Figure 5a, S16 and S17). The key *COOH intermediate was thermodynamically beneficial to form on PT sites to produce CO or CH_4, avoiding the generated *OCHO intermediate of HCOOH product in TPE-PT. Moreover, for the CO product, the stable cyclic carbonate intermediate with a five-membered ring was only found in the TPE-PT, due to the stronger adsorption for *CO intermediate on PT active sites (Figure 5a, b), consistent with *in situ* DRIFTS (Figure 4c), and the follow-up reaction continued to thermodynamically generate CH_4 (Figure S16). However, in TPT-AQ, the weaker interaction between *CO and AQ generated an unstable four-membered ring intermediate, which subsequently released CO and terminated the reaction (Figure 5a, b), and thus the cyclic carbonate species was not observed in Figure 4d. The reaction process of non-sacrificial CO_2 and H_2O conversion to CH_4 and H_2O_2 in metal-free TPE-PT photocatalyst was described in Figure 5c. (1) Under the light irradiation, photo-generated electrons transferred through the alkynyl bridge to O atoms of PT to form oxygen-centered radicals, with holes on TPE. (2) Then, CO_2 and H_2O reactants adsorbed on oxygen-centered radicals (PT) and TPE/alkynyl sites to form *CO_2 and π…HO species, respectively. (3) The formed *COOH and *OH intermediates were on reduction (PT) and oxidation (TPE/alkynyl) sites, respectively. (4) The dehydroxylation of *COOH sites generated the key stable cyclic carbonate with a five-membered ring on PT, leading to less CO product, which was more favorable to the follow-up reaction to thermodynamically generate *CHO, *CH_2O, *CH_3O, CH_3OH, *CH_3 intermediates and the final product of CH_4. (5) For the oxidation reaction, *OH intermediate on C atom (TPE/alkynyl) was oxidized by holes to H_2O_2, and the O_2 from partial H_2O oxidation adsorbed on benzene rings near alkynyl as O_2^- intermediate was further reduced. Due to the different active sites of CO_2 reduction and H_2O oxidation, the available water oxidation capacity to transfer H_2O-H_2O_2, or H_2O-O_2-H_2O, resulted in the needless of hole sacrificial agents and separation of CH_4 from by-product O_2, providing more photo-generated electrons for efficient CO_2 reduction.

Excitonic Dissociation and Electron Transfer

Besides the strong coordination of CO on active sites, more electrons were required for CO_2 photoreduction to the CH_4 product. Therefore, photoluminescence (PL) tests were conducted to compare the excitonic recombination efficiencies of the metal-free organic polymeric materials.[34] The PL emission of TPE-PT exhibited the weakest intensity compared with the TPE-AQ and TPT-AQ (Figure 5d), evidencing that PT was more capable of electron withdrawing than AQ, thus promoting exciton dissociation. Photo-luminescence quenching yield (PLQY) measurements also monitored the overall excitonic recombination efficiencies. The quantum yields were 0.4%, 0.8%, and 0.5% for TPE-PT, TPE-AQ, and TPT-AQ, respectively, one more demonstrating that the geminate charge recombination was completely suppressed in TPE-PT.[35]

The electron transfer after excitonic dissociation was also investigated to confirm the excellent electron withdrawal ability of PT. The intensities of the transient photocurrent responses of TPE-PT were much higher than those of TPE-AQ and TPT-AQ (Figure 5e), indicating the larger amount of charge carriers in TPE-PT. The kinetics for electron utilization was also characterized by fs-TA spectra. Some peaks between 900 and 1200 nm could be assigned to the electron absorption, because of a significant decrease after the addition of $AgNO_3$ (Figure 5f, g and S18).[36] The average lifetimes of electrons were estimated to be 119.7 ps for TPE-PT, and 368.5 ps for TPE-AQ in argon conditions (Figure 5h and S18c). The obviously decreased lifetimes of electrons in TPE-PT may be attributed to the more capable electron withdrawal of PT than AQ mentioned above, which accelerated the electron abstracted by PT. Moreover, the average electron lifetime in TPE-PT was nearly the same in CO_2-saturated compared with argon conditions, which was 161.0 ps (Figure 5i and S19).

Conclusion

A novel metal-free organic active site of PT was designed for highly-selective conversion of CO_2 and H_2O to high combustion-value fuel of CH_4, which was easily separated from the H_2O_2 by-product, under room temperature, renewable solar irradiation, and non-sacrificial sustainable conditions (only water). To our best knowledge, this is the first time that metal-free and non-sacrificial photocatalytic CO_2 and H_2O to CH_4 and H_2O_2 under ambient conditions. In the metal-free system, the PT active sites served as electron-acceptors to conduct the electron D-A photocatalyst achieving highly-selective CH_4 production of 10.6 $\mu mol \cdot g^{-1} \cdot h^{-1}$ and up to 90% electronic selectivity, which was nearly 9 times higher than that of electron-acceptors of AQ. Moreover, TPE-PT exhibited excellent light absorption throughout the visible region to dispense the use of photosensitizer. Furthermore, TPE-PT with more capable electron withdrawal ability of PT demonstrated almost complete exciton dissociation, ultrafast photo-induced electron extraction in 161.0 ps, combined with the available water oxidation capacity to transfer H_2O-H_2O_2 or H_2O-O_2-H_2O, resulted in the needless of hole sacrificial agents and separation of CH_4 from by-product H_2O_2. Importantly, the excited PT activated CO_2 for key *COOH species for initiating the CH_4 production, not the *OCHO intermediate of HCOOH product, and the subsequent formation of stable five-member-ring cyclic carbonate intermediate effectively deceased the free energy of *CO to avoid a release of CO. We believe that the metal-free organic active site for highly-selective photocatalytic methanation provides a new approach to produce and separate high-combustion-value fuel of CH_4.

Acknowledgments

This work was supported by the National Natural Science Foundation of China (Grant 22336007, 22206209, and 22106067, 62375120), and the NSF of Guangdong Province (Grant 2022A1515011953).

Keywords: metal free • photocatalysis • CO_2 reduction • polymer • ambient

[1] C. Hepburn, E. Adlen, J. Beddington, E. Carter, S. Fuss, N. Dowell, J. Minx, P. Smith, C. Williams, *Nature* **2019**, *575*, 87-97.

[2] Y. Tachibana, L. Vayssieres, J. R. Durrant, *Nat. Photonics* **2012**, *6*, 511-518.

[3] U. Ulmer, T. Dingle, P. N. Duchesne, R. H. Morris, A. Tavasoli, T. Wood, G. A. Ozin, *Nat. Commun.* **2019**, *10*, 3169.

[4] J. Wu, Y. Huang, W. Ye, Y. Li, *Adv. Sci.* **2017**, *4*, 1700194.

[5] J. Rongé, T. Bosserez, D. Martel, C. Nervi, L. Boarino, F. Taulelle, G. Decher, S. Bordiga, J. A. Martens, *Chem. Soc. Rev.* **2014**, *43*, 7963-7981.

[6] B. Kumar, M. Llorente, J. Froehlich, T. Dang, A. Sathrum, C. P. Kubiak, *Annu. Rev. Phys. Chem.* **2012**, *63*, 541-569.

[7] J. Ran, M. Jaroniec, S. Z. Qiao, *Adv. Mater.* **2018**, *30*, 1704649.

[8] Y. Zhu, Z. Xu, Q. Lang, W. Jiang, Q. Yin, S. Zhong, S. Bai, *Appl. Catal. B: Environ.* **2017**, *206*, 282-292.

[9] R. Long, Y. Li, Y. Liu, S. Chen, X. Zheng, C. Gao, C. He, N. Chen, Z. Qi, L. Song, J. Jiang, J. Zhu, Y. Xiong, *J. Am. Chem. Soc.* **2017**, *139*, 4486-4492.

[10] S. C. Roy, O. K. Varghese, M. Paulose, C. A. Grimes, *ACS Nano* **2010**, *4*, 1259-1278.

[11] M. Lu, M. Zhang, J. Liu, T. Y. Yu, J. N. Chang, L. J. Shang, S. L. Li, Y. Q. Lan, *J. Am. Chem. Soc.* **2022**, *144*, 1861-1871.

[12] H. Zhang, Y. Wang, S. Zuo, W. Zhou, J. Zhang, X. W. D. Lou, *J. Am. Chem. Soc.* **2021**, *143*, 2173-2177.

[13] L. Ran, Z. Li, B. Ran, J. Cao, Y. Zhao, T. Shao, Y. Song, M. K. H. Leung, L. Sun, J. Hou, *J. Am. Chem. Soc.* **2022**, *144*, 17097-17109.

[14] W. Wang, C. Deng, S. Xie, Y. Li, W. Zhang, H. Sheng, C. Chen, J. Zhao, *J. Am. Chem. Soc.* **2021**, *143*, 2984-2993.

[15] T. Banerjee, F. Podjaski, J. Kröger, B. P. Biswal, B. V. Lotsch, *Nat. Rev. Mater.* **2021**, *6*, 168-190.

[16] S. Barman, A. Singh, F. Rahimi, T. Maji, *J. Am. Chem. Soc.* **2021**, *143*, 16284-16292.

[17] W. Xie, J. Xu, U. MdIdros, J. Katsuhira, M. Fuki, M. Hayashi, M. Yamanaka, M. Kobori, R. Matsubara, *Nat. Chem.* **2023**, *15*, 794-802.

[18] H. Yan, M. Shen, Y. Shen, X. D. Wang, W. Lin, J. Pan, J. He, Y. X. Ye, X. Yang, F. Zhu, J. Xu, J. He, G. Ouyang, *P. Natl. Acad. Sci. USA* **2022**, *119*, e2202913119.

[19] S. Wang, X. Hai, X. Ding, S. Jin, Y. Xiang, P. Wang, B. Jiang, F. Ichihara, M. Oshikiri, X. Meng, Y. Li, W. Matsuda, J. Ma, S. Seki, X. Wang, H. Huang, Y. Wada, H. Chen, J. Ye, *Nat. Commun.* **2020**, *11*, 1149.

[20] Y. X. Ye, J. Pan, Y. Shen, M. Shen, H. Yan, J. He, X. Yang, F. Zhu, J. Xu, J. He, G. Ouyang, *P. Natl. Acad. Sci. USA* **2021**, *118*, e2115666118.

[21] Y. Cao, L. Guo, M. Dan, D. E.Doronkin, C. Han, Z. Rao, Y. Liu, J. Meng, Z. Huang, K. Zheng, *Nat. Commun.* **2021**, *12*, 1675.

[22] L. Cheng, H. Yin, C. Cai, J. Fan, Q. Xiang, *Small* **2020**, *16*, 2002411.

[23] S. Mondal, N.S. Powar, R. Paul, H. Kwon, N. Das, B. M. Wong, S. In, J. Mondal, *ACS Appl. Mater. Interfaces* **2022**, *14*, 771-783.

[24] K. Wang, J. Fu, Y. Zheng, *Appl. Catal. B: Environ.* **2019**, *254*, 270-282.

[25] Y. Zhang, X. Zhi, J. R. Harmer, H. Xu, K. Davey, J. Ran, S. Z. Qiao, *Angew. Chem. Int. Edit.* **2022**, *61*, e202212355.

[26] C. Dong, C. Lian, S. Hu, Z. Deng, J. Gong, M. Li, H. Liu, M. Xing, J. Zhang, *Nat. Commun.* **2018**, *9*, 1252.

[27] X. Chen, C. Peng, W. Dan, L. Yu, Y. Wu, H. Fei, *Nat. Commun.* **2022**, *13*, 4592.

[28] S. C. Shit, N. S. Powar, P. Kalita, R. Paul, S. J. Xu, J. Jung, C. Cho, S. In, J. Mondal, *Chem. Commun.* **2022**, *58*, 13716-13719.

[29] C. Wu, Z. Teng, C. Yang, F. Chen, H. B. Yang, L. Wang, H. Xu, B. Liu, G. Zheng, Q. Han, *Adv. Mater.* **2022**, *34*, 2110266.

[30] X. Zhang, N. A. Vermeulen, Z. Huang, Y. Cui, J. Liu, M. D. Krzyaniak, Z. Li, H. Noh, M. R. Wasielewski, M. Delferro, O. K. Farha, *ACS Appl. Mater. Interfaces* **2018**, *10*, 635-641.

[31] M. P. Kou, Y. Y. Wang, Y. X. Xu, L. Q. Ye, Y. P. Huang, B. H. Jia, H. Li, J. Q. Ren, Y. Deng, J. H. Chen, Y. Zhou, K. Lei, L. Wang, W. Liu, H. W. Huang, T. Y. Ma, *Angew. Chem. Int. Ed.* **2022**, *61*, e202200413.

[32] a) F. A. Rahimi, S. Dey, P. Verma, T. K. Maji, *ACS Catal.* **2023**, *13*, 5969-5978. b) G. H. Feng, S. B. Wang, S. G. Li, R. P. Ge, X. F. Feng, J. W. Zhang, Y. F. Song, X. Dong, J. Z. Zhang, G. F. Zeng, Q. Zhang, G. J. Ma, Y. D. Chuang, X. X. Zhang, J. H. Guo, Y. H. Sun, W. Wei, W. Chen, *Angew. Chem. Int. Ed.* **2023**, *62*, e202218664.

[33] a) J. Y. Yue, L. P. Song, Y. F. Fan, Z. X. Pan, P. Yang, Y. Ma, Q. Xu, B. Tang, *Angew. Chem. Int. Ed.* **2023**, *62*, e202309624. b) F. Y. Liu, P. Zhou, Y. H. Hou, H. Tan, Y. Liang, J. L. Liang, Q. Zhang, S. J. Guo, M. P. Tong, J. R. Ni, *Nat. Commun.* **2023**, *14*, 4344.

[34] J. Kosco, M. Bidwell, H. Cha, T. Martin, C. T. Howells, M. Sachs, D. H. Anjum, S. Gonzalez Lopez, L. Zou, A. Wadsworth, W. Zhang, L. Zhang, J. Tellam, R. Sougrat, F. Laquai, D. M. DeLongchamp, J. R. Durrant, I. McCulloch, *Nat. Mater.* **2020**, *19*, 559-565.

[35] M. Madhu, R. Ramakrishnan, V. Vijay, M. Hariharan, *Chem. Rev.* **2021**, *121*, 8234-8284.

[36] J. Ma, T. J. Miao, J. Tang, *Chem. Soc. Rev.* **2022**, *51*, 5777-5794.

10.1002/anie.202313392

Entry for the Table of Contents

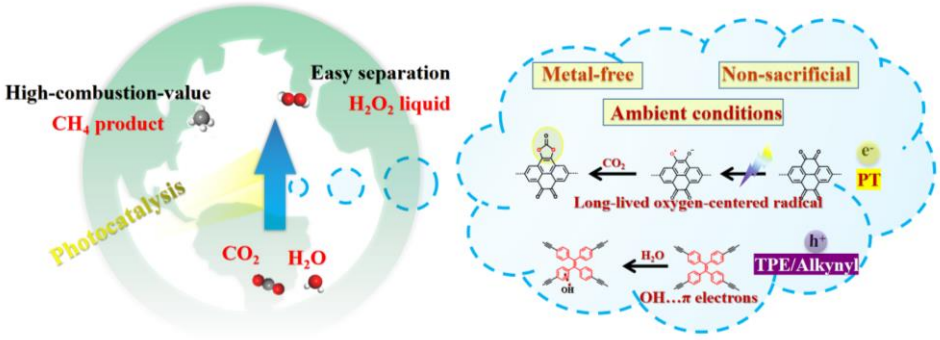

A metal-free photocatalyst achieves high electronic selectivity for CH_4 and facile separation of H_2O_2 in non-sacrificial ambient conditions with only CO_2 and H_2O. This exceptional performance is attributed to a long-lived oxygen-centered radical in the excited electron acceptor, promoting the formation of a stabilized five-member-ring cyclic intermediate with lower energy, leading to an 90% selectivity for the eight-electron product CH_4.